Papers in Physics, vol. 16, art. 160002 (2024)

www.papersinphysics.org

Received: 24 July 2024, Accepted: 12 September 2024
Edited by: B. Vohnsen

DOI: https://doi.org/10.4279/PIP.160002

ISSN 1852-4249

Optoelectronic tuning of Barium titanate doped with Pt: A systematic first-principles study

Mariam Q. Saadon[1], Hussein A. Miran[1*]

In this study, the structural, electronic and optical characteristics of Platinum (Pt)-doped cubic $BaTiO_3$ perovskite were inspected via density functional theory (DFT) calculations. Generalized gradient approximation (GGA) and Pedraw–Wang 91 (PW91) functional, as applied in CASTEP code, provide an atomic level understanding of the influence of substituting 0.125 Pt dopant at Ba and Ti positions. Results indicate that the optimized lattice parameters and band gap are in good agreement with the experimental and theoretical data. Furthermore, the total and projected density of states (TPDOSs) analysis demonstrates that Pt–dopant integration has an impact on diminishing the band gap and shifting the absorption spectra towards the visible light region. Thus, it is suggested that substituting Ti and Ba atoms with Pt would enhance the optoelectronic characteristics of the host system, due to existing Pt–5d electronic states. Moreover, the negative formation energy values indicate the thermodynamic stability of the modeled configurations. These detailed results provide valuable insights into the physical properties of Pt–$BaTiO_3$ and its behavior across a range of photon wavelengths. To our knowledge, this contribution evaluates for the first time the influence of introducing platinum (Pt) into a $BaTiO_3$ perovskite system. The overall findings demonstrate a valuable appraisal of support for experimental synthesis of Pt–$BaTiO_3$ to serve in various optoelectronic devices.

I Introduction

The recent development of materials engineering with controlled characteristics is of pronounced significance [1–7]. Oxide perovskites with the form ABO_3, where A and B correspond to the cations (metals), and O signifies the anion (Oxygen), have emerged as an interesting class of materials in various industrial and technological applications, for instance, in photovoltaic devices, ferroelectrics, solar panels, and catalysts [8–10]. The band gap is fundamentally associated with charge shifting from O–2p orbitals situated within the valence band to d orbitals of the transition metals located in the conduction band [11]. It has been reported that a minor percentage of solar radiation, of approximately 5%, would be absorbed within the UV spectrum [12, 13]. Thus, it is recommended to adjust the band gap of $BaTiO_3$ to stretch the photo response toward the visible region [14]. In order to augment the optical absorption characteristics of $BaTiO_3$, a doping strategy was adopted to create a novel acceptor or donor level in the valance and conduction energy bands [15]. The key point of utilizing $BaTiO_3$ perovskites in photovoltaic applications comprises the remarkable photovoltaic influence produced by brilliant ferroelectric behavior [16]. In addition, they provide a broad range of possibilities for switchable constituents by dopant-

* hussein.a.j@ihcoedu.uobaghdad.edu.iq

[1] Department of Physics, College of Education for Pure Science, Ibn Al-Haitham, University of Baghdad, Baghdad, Iraq.

introduction at Ba or Ti positions for controlling their electronic, electrical and optical characteristics [17–19]. Furthermore, the synthesis procedures involve cost effective equipment such as spray pyrolysis, sol-gel, and magnetron sputtering [20]. Significant numbers of investigations have been dedicated to understanding the effective impact of dopants on enhancing diverse properties of the pristine $BaTiO_3$ and reducing dielectric loss [21–27]. Although doping represents an effective strategy for tailoring required materials for diverse technological and industrial fields, controlling the cation arrangement remains a substantial feat still needing to be achieved. Cadmium (Cd)- accommodated at Ba position of $BaTiO_3$ has an impact on narrowing the band gap and improving the optical properties, which could serve in various electronic industries [28]. Strontium (Sr) inclusion at the Pb lattice of $PbTiO_3$ cubic perovskite could reduce the band gap and shift the optical response by lowering refractive index and increasing absorption in the visible region [29].

Pt quantum dots-doped $La_2Ti_2O_7$ nanosheets have been synthesized using the hydrothermal approach [30]. Alongside, density functional theory (DFT) calculations were used to analyze the effect of Pt doping for discriminating NO elimination and evading the NO_2 secondary contaminant. It has been established that Pt atom integration over $La_2Ti_2O_7$ surfaces would reduce the band gap of these surfaces, in turn expanding its light absorption coverage in the visible-light region, since Pt atoms perform as bridges to expedite the charge carrier transfer [31]. In another study, $La_2Ti_2O_7$ nanosheets modified by Pt quantum dots were prepared for efficient NO removal avoiding the NO_2 secondary contaminant [32]. $NiTiO_3$ and $ZnTiO_3$ perovskite nanostructures were prepared via the hydrothermal procedure, adding 1 wt% of Pt to attain Pt–$NiTiO_3$ and Pt–$ZnTiO_3$. The results demonstrated that Pt-loading improved the material sensitivity and induced Pt–$NiTiO_3$ selectivity towards NO_2, compared to more harmful pollutants such as CO_2 and SO_2 [33]. A recent contribution has investigated the impact of substituting 0.125 Palladium (Pd) dopant at Ba and Ti positions on enhancing the photocatalytic activities of $BaTiO_3$ [34]. To our knowledge, this contribution evaluates for the first time the influence of introducing Pt into a $BaTiO_3$ perovskite system: the impact of Pt inclusion on the physical properties of Barium titanate was evaluated. The attained results would provide a useful guide for tailoring a Pt-based efficient light absorber using the state-of-the-art density functional theory (DFT). The current paper is structured as follows: Section 1 introduces the most cited literature. Section 2 highlights the computational methodology approach. Section 3 covers results and discussion, interpreting and analyzing the attained results. Finally, Section 4 draws conclusions from the study and presents the key findings and outlook.

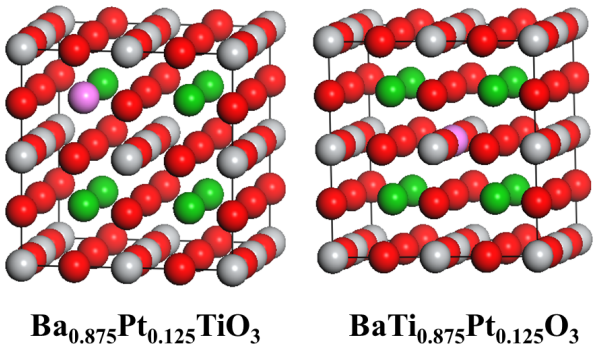

Figure 1: The optimized 2×2×2 supercells of the modeled configurations. Green, Gray, pink, and red spheres denote, Ba, Ti, Pt, and O atoms, respectively.

II Calculation methodology

The examination of Pt–doped $BaTiO_3$ was performed by means of first-principles calculations by implementing the supercell method. Investigation of the electronic structure was carried out using the state-of-the-art density functional theory (DFT), as executed in Cambridge Serial Total Energy Package (CASTEP) [35, 36]. The projector-augmented wave function (PAW) approach within the generalized gradient approximation (GGA-PW91) was applied for the exchange-correlation energy [37, 38]. The energy cutoff was set as 300 eV and the Brillouin-zone (BZ) was sampled by Monkhorst-Pack k meshes [39]corresponding to 4×4×4 for both pure $BaTiO_3$ and Pt–doped $BaTiO_3$. The relaxation of the electronic excitation is smaller than 0.01 eV/Å. Moreover, to overcome the intrinsic

Table 1: An evaluation of the ground state properties of pristine and Pt-doped $BaTiO_3$.

The studied configurations	Lattice constants (Å) a=b=c	Formation energy (eV)	Bandgap energy (eV)
Pristine-$BaTiO_3$	4.07 4.03	-8.55	3.21 3.19
$Ba_{0.875}Pt_{0.125}TiO_3$	4.02	-8.44	1.78
$BaTi_{0.875}Pt_{0.125}O_3$	4.04	-8.31	2.06

drawback of the underestimation of the DFT approach, a scissor operator value of about 0.75 eV was systematically utilized to estimate the experimental energy band gap [40]. In the current simulation study, an original unit cell of $BaTiO_3$ was optimized first, then a 2×2×2 supercell consisting of 40 atoms (i.e. 8 atoms of Ba^{2+}, 8 atoms of Ti^{4+}, and 24 atoms of O) was constructed. The considered loaded ratio of Pt dopant corresponds to 0.125. In order to consider such a content, two categories were implemented in which one atom of Ba^{2+} (in case of occupying Ba site) or one Ti^{4+} (in case of occupying Ti site) has been substituted with a Pt atom. Furthermore, the formation energy of the pure $BaTiO_3$ was assessed and expressed as below [34, 41]:

$$\Delta E_{f_{BaTiO_3}} = \frac{1}{x+y+z}(E_{sum(BaTiO_3)} - xE_{Ba} - yE_{Ti} - zE_o). \quad (1)$$

Herein, x, y and z are fixed numbers representing the atomic molar ratios of Ba, Ti, and O, respectively.

In addition, the formation energies of $Ba_{0.875}Pt_{0.125}TiO_3$ and $BaTi_{0.875}Pt_{0.125}O_3$ systems are expressed as below:

$$\Delta E_{fBa_{0.875}Pt_{0.125}TiO_3} = \frac{1}{x+m+y+z}(E_{sum(Ba_{0.875}Pt_{0.125}TiO_3)} - xE_{Ba} - mE_{Pt} - yE_{Ti} - zE_o), \quad (2)$$

$$\Delta E_{f_{BaTi_{0.875}Pt_{0.125}O_3}} = \frac{1}{x+y+m+z}(E_{sum(BaTi_{0.875}Pt_{0.125}O_3)} - xE_{Ba} - yE_{Ti} - mE_{Pt} - zE_o). \quad (3)$$

where x,y,z, and m symbolize the molar portion of Ba, Ti, O, and Pt atoms, correspondingly.

For evaluating the dopant formation energy of Pt-insertion into the host lattice of $BaTiO_3$, the following relationship is utilized [42],

$$E_f = E_{Pt-doped} - [E_{host\ lattice} - (\mu_{Ba} \text{ or } \mu_{Ti}) + \mu_{Pt}]. \quad (4)$$

wherein E_f refers to the formation energy of the Pt-dopant and $E_{host\ lattice}$ corresponds to the energy of the pristine system. μ_{Ba}, μ_{Ti} and μ_{Pt} signify the chemical potential of Ba, Ti and Pt atoms, respectively. The chemical potentials of these atoms correspond to the energies of the species in their solid lattice (the doped modeled supercells). In the case of Pt insertion at Ba and Ti sites, the energy of μ_{Ba} or μ_{Ti} are fulfilled, correspondingly. The required formation energy of the Pt atom to be situated at the Ba position is determined as 4.17 eV, while the required formation energy of Pt at the Ti site satisfies 9.56 eV. Thus, the preference of the Pt atom to accommodate at Ba is more applicable than at the Ti site.

III Results and discussion

i Electronic properties, geometrical relaxation, and stability evaluations

Literature has stated that Ba and Ti sites with coordination numbers of 12 and 6, respectively, play a certain role in engineering the desired optoelectronic characteristics of $BaTiO_3$ via substitution at those sites. The modeled $BaTiO_3$ system crystalizes in cubic phase (Pm-3m 221) in which Ti, Ba, and O atoms accommodate at Wyckoff positions of $(0,0,0)$, $(0.5,0.5,0.5)$, and $(0.5,0.5,0)$, respectively [43]. Platinum (Pt) is a transition metal with

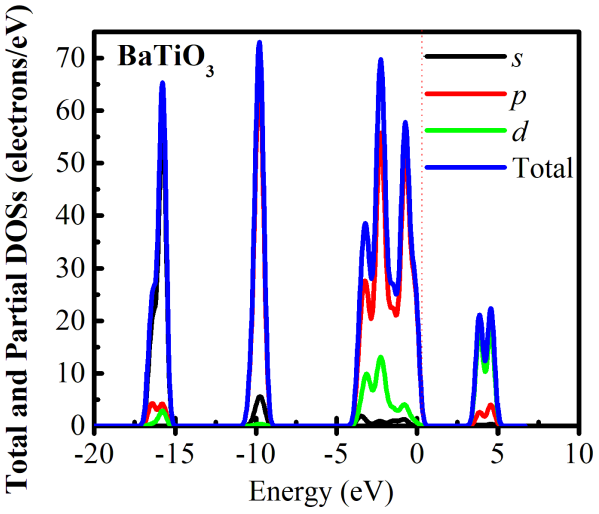

Figure 2: The total and partial density of states for pure $BaTiO_3$ system. The dashed line corresponds to the Fermi level.

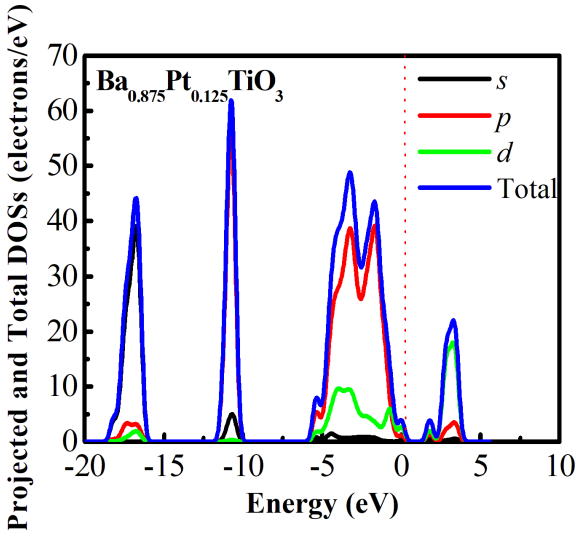

Figure 3: The total and partial density of states for $Ba_{0.875}Pt_{0.125}TiO_3$. The dashed line corresponds to the Fermi level.

an atomic number 78. Its electron configuration is [Xe] $4f^{14}$ $5d^9$ $6s^1$. Fig. 1 displays the crystal structures of Pt-doped $BaTiO_3$.

The predicted bandgap energy and lattice constants of $BaTiO_3$ are reported, and demonstrated an agreement between experimental and theoretical studies [44–46]. Table 1 displays the formation energies of pristine and doped $BaTiO_3$. A negative formation energy value suggests that a system is thermodynamically stable and can experimentally be synthesized, while a positive value indicates instability of the system. It is noticeable that the pristine and doped systems exhibit negative values and approximately equivalent stability. Moreover, it is critical to ascertain structural stability of all components. The integration of Pt into $BaTiO_3$ implies a trivial reduction in the overall stability.

As reported earlier in literature, $BaTiO_3$ exhibits a non-metallic nature indicating a semiconducting behavior [47]. The electronic properties of a $BaTiO_3$ unit cell is inspected by analyzing the total and projected density of states (TPDOSs) of the relaxed configuration. The states of TPDOSs for the studied structure of $BaTiO_3$ are presented in Fig. 2. The valence band shown in Fig. 2 prominently comprises O – 2p peaks with minor contributions from Ba – 4d and Ti – 3d states. However, the conduction band is mostly composed of Ba – 4d and Ti – 3d states. The estimated bandgap of the pristine discloses a magnitude of 3.21 eV, which is in accordance with the parallel experimental value [44].

Concerning the doped configurations shown in

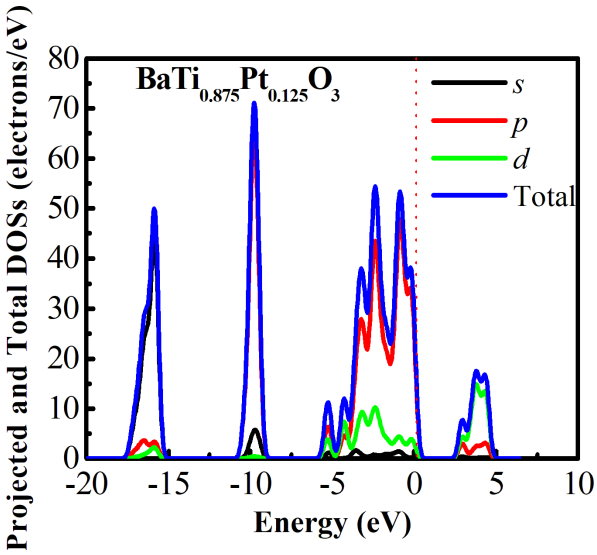

Figure 4: The total and partial density of states of $BaTi_{0.875}Pt_{0.125}O_3$ configuration. The dashed line corresponds to the Fermi level.

Table 2: The predicted charge distribution results of pristine $BaTiO_3$.

Atoms	s	p	d	Total charge (e)	Charge transfer (e)
O	1.98	5.02	0.00	7.01	-1.01
Ti	2.32	5.81	2.28	10.41	1.59
Ba	1.98	6.00	0.67	8.56	1.44

Figs. 3 and 4, it can be obviously seen that VB is principally initiated from O – 2p with a slight involvement of Ba – 4d, Ti – 3d, and Pt – 5d,whereas the majority of CB comprises d states and the minority corresponds to p states. Fig. 3 portrays the electronic projected (partial) and total density of states for Pt–doped $BaTiO_3$ at the Ba site. This figure indicates that the Pt – 5d orbital is situated at 1.78 eV from Fermi level (0 eV), having a firm hybridization with O – 2p orbitals. On the other hand, the p – d hybridization resulted in reducing DOSs of the valance bands. Fig. 4 depicts PDOSs and TDOSs for Pt–included $BaTiO_3$ at the Ti site. In this case, Pt – 5d orbital is positioned at 2.06 eV from Fermi level with having a robust hybridization with O – 2p states.

Remarkably, the introduction of a Pt atom positioned at Ba and Ti sites lead to reducing the bandgap value to 1.78 eV and 2.06 eV, respectively, signifying a semiconducting trend as documented in Table 1. It is also worth reporting the indication that the energy band gap window lies slightly above the Fermi level. This could be justified by the instability in magnetic properties due to the high density of states of the studied materials. The reduction of the band gap energy during Pt insertion is originated from the emergence of electronic states in the gap between valance and conducting bands [48].

From another perspective, carrying out spin polarized calculations demonstrates quite similar density of states and band gap values for the explored systems, as depicted in Figs. 5 to 7.

Furthermore, Pt–doped configurations displayed a magnetic property which is originated from inserting Pt into $BaTiO_3$ which reveals its ferromagnetism [49]. Band gap schemes of pristine and Pt– doped $BaTiO_3$ have been plotted in Figs. 8 to 10. The figures display strong hybridization owing to introducing Pt-5d orbitals, as explained in TPDOSs plots.

Appraising charge density distribution provides an assessment of the bonding nature. Mulliken population analysis is of great use when evaluating charge distribution. Furthermore, it offers insight into the sort of bonding involved (i.e. ionic and covalent bonds): Mulliken charge population value amounts to zero for ideal ionic bonds, whereas it corresponds to unity for perfect covalent bonds [50]. Mulliken population was performed in CASTEP by applying a projection of the plane wave basis set onto a localized basis using a modified method established by Sanchez-Portal et al. [51]. Table 2 reports Mulliken charges of pristine and Pt-doped $BaTiO_3$. The Mulliken population illustrates that the covalency and ionic strength of the bond can be estimated.

A high population magnitude designates covalent bonding, whereas a low magnitude indicates an ion-interacting bond. Impurities would influence the adjacent atoms [52–54]. The Ti–O bonds hold non-zero positive values, favoring the ionic and covalent trends in all the compounds evaluated. Accordingly, the incorporation of the Pt ion into the pristine system results in a rise of the covalence behavior of Ba–O and Ti–O bonds, accompanied by a reduction in the ionicity. The ionic bonding is undoubtedly aligned with the charge reassigning between atoms in molecules. The moderately negative charge of O and positive charges of Ba, Ti and Pt atoms, correspondingly, favor more charge accumulating around O atoms, which is demonstrated in charge gaining [55]. In turn, less charge accumulating around Ba, Ti and pt atoms implies charge

Table 3: The predicted atomic Mulliken populations and bond length (Å) of pristine $BaTiO_3$.

Bonds	Mulliken populations	Bond length (Å)
O-Ti	0.26	2.04
O-O	-0.06	2.87
O-Ba	-0.27	2.87

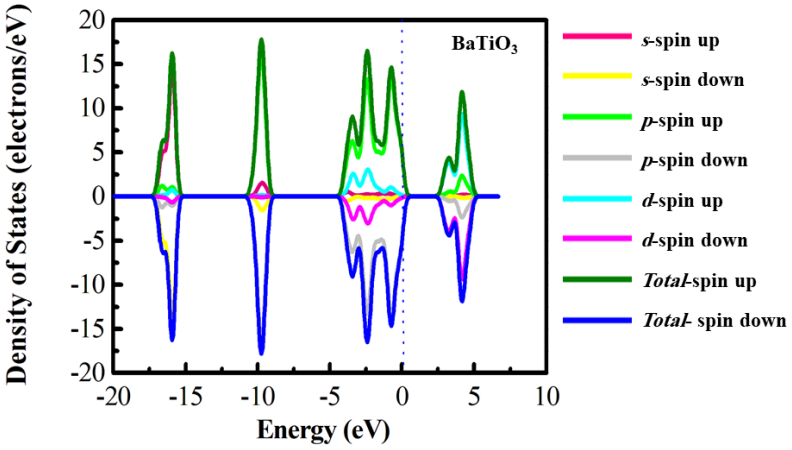

Figure 5: Spin polarized density of states of $BaTiO_3$.

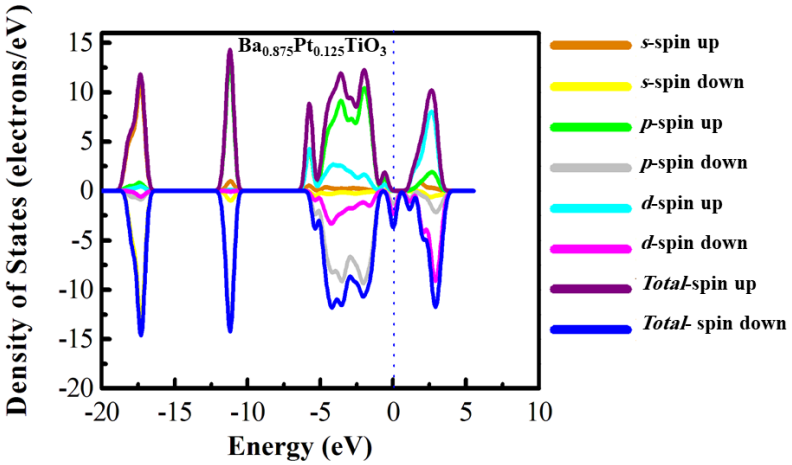

Figure 6: Spin polarized density of states of $Ba_{0.875}Pt_{0.125}TiO_3$.

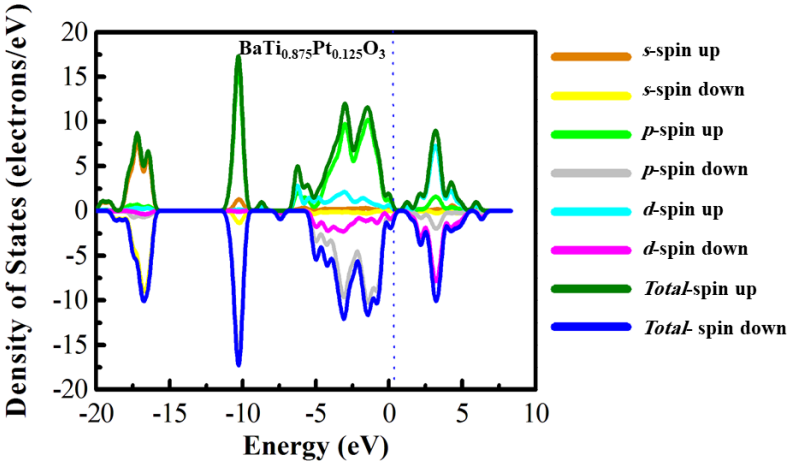

Figure 7: Spin polarized density of states of $BaTi_{0.875}Pt_{0.125}O_3$.

Table 4: The assessed charge distribution results of $Ba_{0.875}Pt_{0.125}TiO_3$.

Atoms	s	p	d	Total charge (e)	Charge transfer (e)	Magnetic moment (hbar)
O	1.95	4.98	0.00	6.93	-0.93	0.13
Ti	2.30	5.94	2.30	10.53	1.60	0.14
Ba	1.88	6.01	0.69	8.58	1.45	0.03
Pt	0.62	0.32	8.69	9.64	0.36	0.89

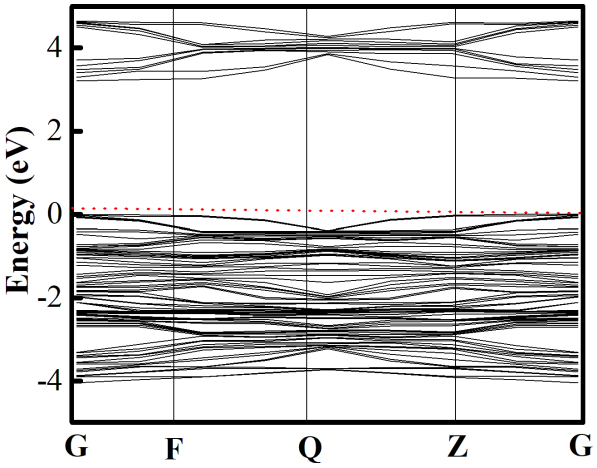

Figure 8: Band gap scheme of pristine BaTiO3.

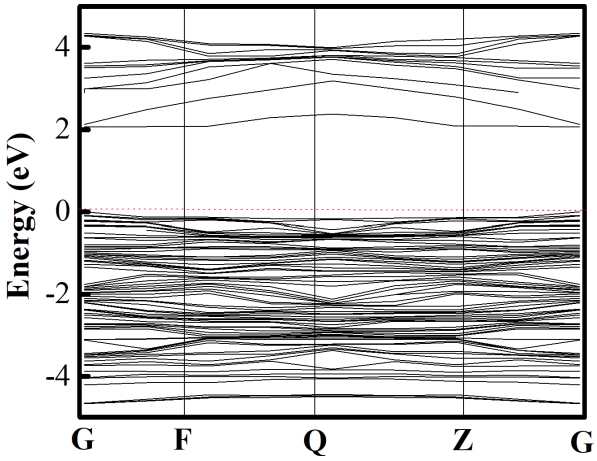

Figure 10: Band gap scheme of $BaTi_{0.875}Pt_{0.125}O_3$.

reduction. This is owing to the fact that O atoms hold electronegativity values greater than Ba, Ti and Pt atoms.

Moreover, Table 2 portrays negative charges for O atoms with reference to the ionic tendency between anions and cations in the structures in question. Therefore, substitution at Ba and Ti atomic sites by a Pt atom sees plummets in their charge values. Nonetheless, further charges show growth around O atoms when cation sites are replaced by Pt atoms. Tables 3 to 7 display the atomic Mulliken populations and bond length (Å) of pristine $BaTiO_3$ and Pt substituted at Ba/Ti sites of $BaTiO_3$. Increasing the positive value of the Mulliken charge for Ba and Ti ions in the studied compounds can be understood based on the sturdier mixture with surrounding oxygen ions, when the

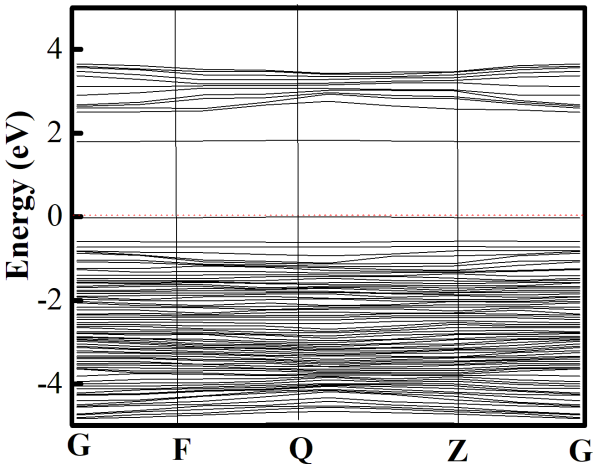

Figure 9: Band gap scheme of $Ba_{0.875}Pt_{0.125}TiO_3$.

Table 5: The estimated atomic Mulliken populations and bond length (Å) of $Ba_{0.875}Pt_{0.125}TiO_3$.

Bonds	Mulliken populations	Bond length (Å)
O-Ti	0.25	1.89
O-O	-0.05	2.85
O-Ba	-0.36	2.82
O-Pt	0.10	2.46

Table 6: Charge distribution data of $BaTi_{0.875}Pt_{0.125}O_3$.

Atoms	s	p	d	Total charge (e)	Charge transfer (e)	Magnetic moment (hbar)
O	1.98	5.03	0.00	7.01	-1.01	0.28
Ti	2.33	5.74	2.29	0.34	1.65	0.05
Ba	1.85	6.00	0.66	8.52	1.48	0.01
Pt	0.76	0.05	8.12	8.93	1.07	0.97

negative charge is shifted towards oxygen ions [56]. Based on the attained charge transfer results, it can be concluded that the bonding character of Pt–$BaTiO_3$ is a mixture of covalent and ionic in nature.

Table 7: Atomic Mulliken populations and bond length (Å) of $BaTi_{0.875}Pt_{0.125}O_3$.

Bonds	Mulliken populations	Bond length (Å)
O-Ti	0.24	2.03
O-O	-0.06	2.86
O-Ba	-0.27	2.82
O-Pt	0.10	2.09

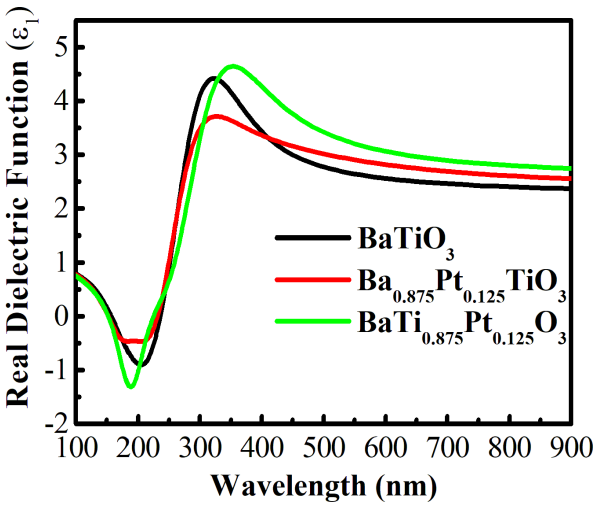

Figure 11: The estimated real dielectric component spectra of pristine $BaTiO_3$,$BaTi_{0.875}Pt_{0.125}O_3$, and $Ba_{0.875}Pt_{0.125}TiO_3$ structures.

ii Optical properties

It has been reported that the dielectric function is a critical feature showing the absorption and polarization properties of materials [57, 58]. The real part(ε_1) designates the quantity of a substance being polarized when electromagnetic waves are penetrating it. The dielectric component is composed of real and imaginary parts, as given below [59, 60]:

$$\varepsilon(\omega) = \varepsilon_1(\omega) + i\varepsilon_2(\omega). \tag{5}$$

The inspected real dielectric constant of pristine and Pt-doped $BaTiO_3$ are illustrated in Fig. 11. It can be obviously concluded that incorporation of Pt atoms into the host system improves the dielectric constant in the visible region, especially with Pt positioned at the Ti site. Negative values of the real dielectric constant in the range of roughly $150-250$ nm for the spectra are attributed to overshooting the resonance frequency value in the material [61]. This resonance occurs owing to the rotation of the ions or electrons spinning in the material. Moreover, the nonzero values of the imaginary component of the dielectric constant are revealed in Fig. 12, which designates the proceeding of absorption in that energy region. To benchmark the influence of conducting spin polarization assessment on the optical characteristics, real and imaginary components of dielectric function have been obtained. Figs. 13 and 14 correspond to spin-polarized real and imaginary dielectric constants. The reason for the shifting of spin-polarization and non-spin polarization of real and imaginary dielectric spectra is justified by the electronic spin interactions. The reflectivity of pure and Pt– doped $BaTiO_3$ versus wavelength is demonstrated in Fig. 15.

The figure indicates that Pt integrated into $BaTiO_3$ reveals enhanced reflectivity values in the ultra-violet region with reference to pure $BaTiO_3$. Furthermore, the $BaTi_{0.875}Pt_{0.125}O_3$ spectrum, compared with that of $Ba_{0.875}Pt_{0.125}TiO_3$, reveals

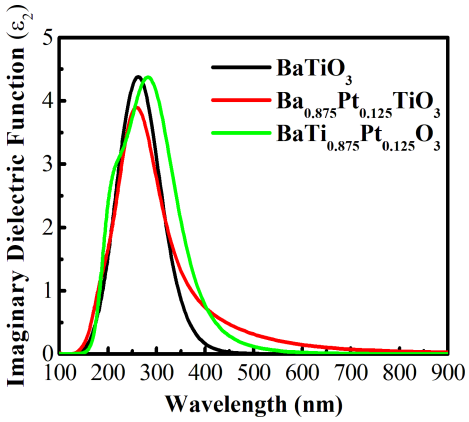

Figure 12: The apprised imaginary dielectric component of pristine $BaTiO_3$,$BaTi_{0.875}Pt_{0.125}O_3$, and $Ba_{0.875}Pt_{0.125}TiO_3$ structures.

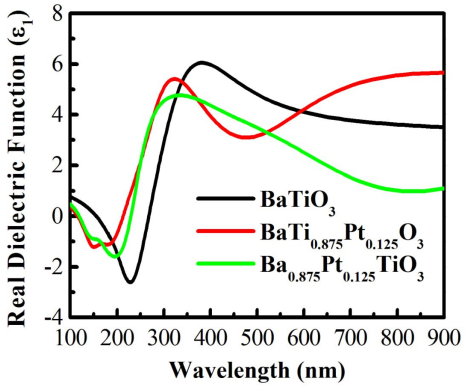

Figure 13: Spin-polarized real dielectric component of pristine $BaTiO_3$,$BaTi_{0.875}Pt_{0.125}O_3$, and $Ba_{0.875}Pt_{0.125}TiO_3$ structures.

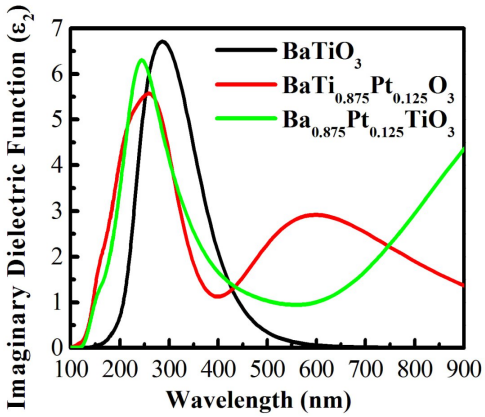

Figure 14: Spin-polarized imaginary dielectric component of pristine $BaTiO_3$,$BaTi_{0.875}Pt_{0.125}O_3$, and $Ba_{0.875}Pt_{0.125}TiO_3$ structures.

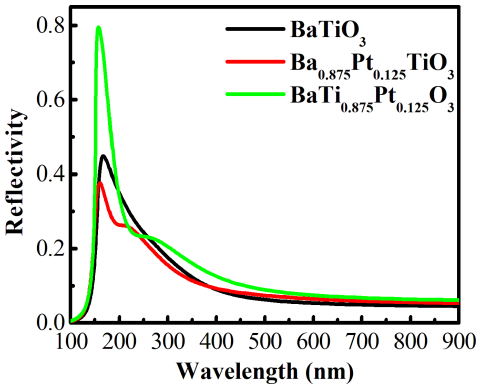

Figure 15: The evaluated reflectivity spectra of pristine $BaTiO_3$,$BaTi_{0.875}Pt_{0.125}O_3$, and $Ba_{0.875}Pt_{0.125}TiO_3$ structures.

a remarkable tendency to reflect the incident photons in the visible array of solar radiation [62, 63]. The variation of real and imaginary components of conductivity with regard to photon wavelength are schemed in Figs. 16 and 17, respectively.

The conductivity of a material designates the capability to transfer electronic charges throughout that material. From these aforementioned diagrams, introducing Pt stimulates an enhanced trend toward visible spectra, demonstrating that this material is opportune for photovoltaic devices [64]. Thus, the refractive index $n(\omega)$ and the extinction coefficient $k(\omega)$ were studied. Figs. 18 and 19 portray the refractive index (real part) and extinction coefficient (imaginary part) of pure $BaTi_{0.875}Pt_{0.125}O_3$ and $Ba_{0.875}Pt_{0.125}TiO_3$ structures. The real part of the refractive index represents the refractive constant of the obtained curves, demonstrating advancement in the visible range,whereas the extinction coefficient, exemplifying the absorbance, reveals that an enhancement is obtained as the Pt atom inserts into the host matrix in the visible range of EMW. On the other hand, assessing the energy loss function for engi-

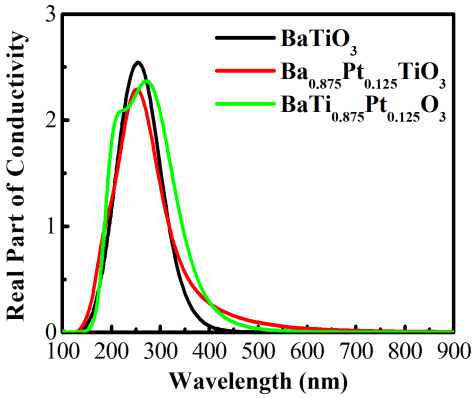

Figure 16: The attained real part of conductivity spectra of pristine $BaTiO_3$,$BaTi_{0.875}Pt_{0.125}O_3$, and $Ba_{0.875}Pt_{0.125}TiO_3$ structures.

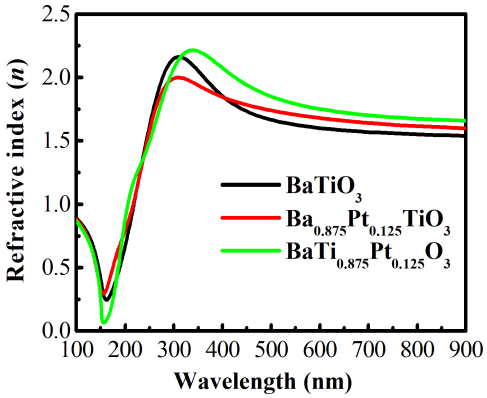

Figure 18: The considered refractive index spectra of pristine $BaTiO_3$,$BaTi_{0.875}Pt_{0.125}O_3$, and $Ba_{0.875}Pt_{0.125}TiO_3$ structures.

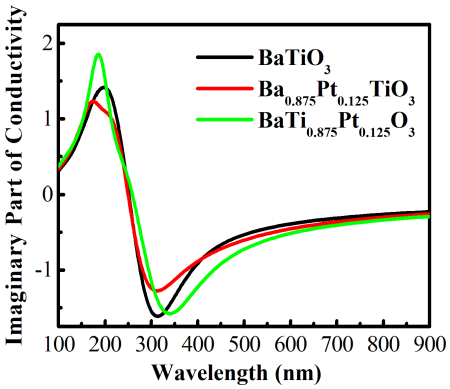

Figure 17: The intended imaginary part of conductivity spectra of pristine $BaTiO_3$, $BaTi_{0.875}Pt_{0.125}O_3$, and $Ba_{0.875}Pt_{0.125}TiO_3$ structures.

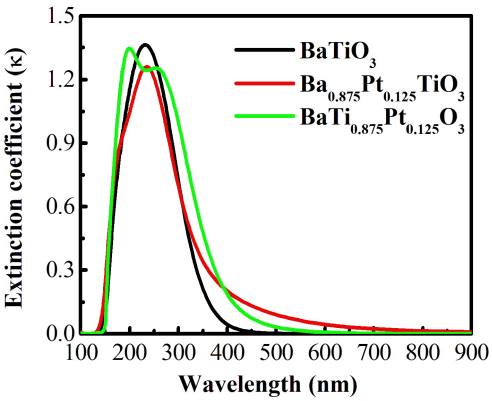

Figure 19: The considered extinction coefficient spectra of pristine $BaTiO_3$,$BaTi_{0.875}Pt_{0.125}O_3$, and $Ba_{0.875}Pt_{0.125}TiO_3$ structures.

neering photoelectric devices is crucial in order to determine the energy loss of the fast electron penetrating a substance. Fig. 20 divulges the loss function spectra of the investigated configurations. It is markedly confirmed that the loss function exhibits a predominant peak at around 200 nm, thereafter diminishing to zero values. Our simulated systems clearly manifest zero values for broad electromagnetic wavelengths, thus nominating them to be non-energy dissipative materials apt to be employed in various optoelectronic devices. In the case of Ti replaced by Pt, it is noticeable that the energy dissipation at nearly 150 nm is much higher than that of other both systems. Finally, the absorption coefficients specify how far light of a certain energy or wavelength is able to enter the substance before absorption [65]. The absorption spectra of the modelled configurations are considered in Fig. 21. A semiconducting trend is clearly observed, since the spectra initiates at a non-zero point of wavelength. Conversely, the spectrum of Pt integrated at the Ti site demonstrated a remarkable enhancement of absorption.

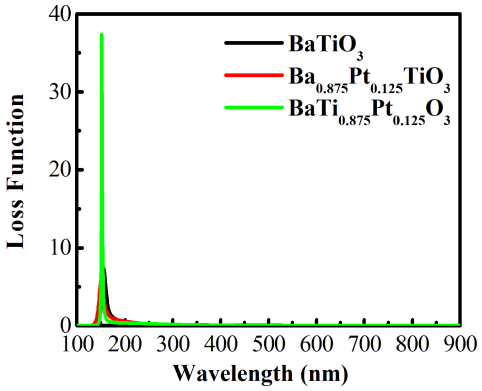

Figure 20: The deliberated loss function spectra of pristine $BaTiO_3$, $BaTi_{0.875}Pt_{0.125}O_3$, and $Ba_{0.875}Pt_{0.125}TiO_3$ structures.

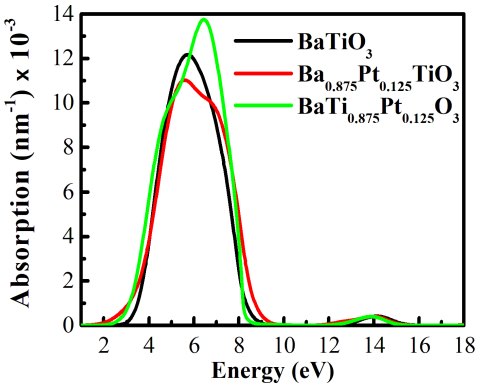

Figure 21: The assessed absorption spectra of pristine $BaTiO_3$, $BaTi_{0.875}Pt_{0.125}O_3$,and $Ba_{0.875}Pt_{0.125}TiO_3$ structures.

IV Conclusions

In summary, the main theme of the current study is to investigate the influence of introducing 0.125 Pt on the ground state properties of $BaTiO_3$ perovskites. The ascertained consequences have recommended that Pt integration into $BaTiO_3$ would diminish the band gap to 1.78 eV and 2.06 eV as it accommodates at Ba and Ti sites, respectively. Furthermore, incorporating Pt–dopant would introduce 5 d states in the conduction band of $BaTiO_3$. The 5 d states demonstrate a substantial upshot on declining the band gap. Moreover, the absorption region of Pt–$BaTiO_3$ is shifted from ultraviolet towards the visible spectra subsequentsoly to Pt integration,implying that the optical absorption is extended toward longer wavelengths (a red-shift). Mulliken's charge distribution exhibited an ionic chemical bonding of Ba–O and Ti–O; however, Ba–Pt and Ti–Pt bonds revealed covalent bonding characteristics. The current outcomes imply that Pt–doped $BaTiO_3$ is a promising material that could serve in photocatalysis applications, as well as demonstrating advantageousness in other diverse optoelectronic technologies. For future work, it would be of great interest to conduct some surface investigations to probe the ability of Pt-$BaTiO_3$ to decompose harmful molecules.

Acknowledgements - The authors acknowledge the support of the university of Baghdad.

[1] Z. N. Jaf, H. A. Miran, Z. T. Jiang, M. Altarawneh, *Molybdenum nitrides from structures to industrial applications*, Rev. Chem. Eng., **39**(3), 329-361, (2023).

[2] Z. N. Jaf, M. Altarawneh, H. A. Miran, Z.-T. Jiang, *Geometries, electronic properties and stability of molybdenum and tungsten nitrides low-index surfaces*, Mater. Res. Express, **5**(12), 126402, (2018).

[3] H. A. Miran, M. Altarawneh, Z. N. Jaf, B. Z. Dlugogorski, Z.-T. Jiang, *Structural, electronic and thermodynamic properties of bulk and surfaces of terbium dioxide (TbO_2)*, Mater. Res. Express, **5**(8), 085901, (2018).

[4] D. S. Shaker, N. K. Abass, R. A. Ulwali, *Preparation and study of the structural, morphological and optical properties of pure tin oxide nanoparticle doped with Cu*, Baghdad Sci. J., **19**(3), 0660-0660, (2022).

[5] M. A. Abood, B. A. Hasan, *A comparison study the effect of doping by Ga_2O_3 and CeO_2 on the structural and optical properties of SnO_2 thin films*, Iraqi J. Sci., 1675-1690, (2023).

[6] H. D. Awad, R. A. Al Anssari, A. H. R. Al-Sarraf, *A study of the structural and optical properties of SnS:F prepared by chemical spray pyrolysis technique*, Baghdad Sci. J., **11**(2), 518-526, (2014).

[7] S. A. Hamdan, *Characterization study of neodymium doped tin oxide films for optoelectronic applications*, Iraqi J. Sci., 2479-2489, (2024).

[8] M. Rizwan, H. M. Naeem Ullah, S. S. A. Gillani, M. Farman, Z. Usman, Z. ur Rehman, *Computational systematic study of pressure driven changes in electronic, optical, elastic, mechanical, thermodynamic and thermoelectric properties of $CaZrO_3$ for optoelectronic and thermoelectric applications*, J. Phys. Chem. Solids, 112150, (2024).

[9] M. Abaid Ullah, M. Rizwan, K. N. Riaz, *Innovative complex perovskites for efficient hydrogen evolution: A DFT-based design strategy*, Mater. Sci. Eng. B, **301**, 117195, (2024).

[10] J. Gao, D. Xue, W. Liu, C. Zhou, X. Ren, *Recent progress on $BaTiO_3$-based piezoelectric ceramics for actuator applications*, Actuators, **6**(3), 24, (2017).

[11] A. Boubaia, A. Assali, S. Berrah, H. Bennacer, I. Zerifi, A. Boukortt, *Band gap and emission wavelength tuning of Sr-doped $BaTiO_3$ (BST) perovskites for high-efficiency visible-light emitters and solar cells*, Mater. Sci. Semicond. Process., **130**, 105837, (2021).

[12] F. Yang, S. Lin, L. Yang, J. Liao, Y. Chen, C.-Z. Wang, *First-principles investigation of metal-doped cubic $BaTiO_3$*, Mater. Res. Bull., **96**, 372-378, (2017).

[13] I. Grinberg, D. V. West, M. Torres, G. Gou, D. M. Stein, L. Wu, G. Chen, E. M. Gallo, A. R. Akbashev, P. K. Davies, et al., *Perovskite oxides for visible-light-absorbing ferroelectric and photovoltaic materials*, Nature, **503**(7477), 509-512, (2013).

[14] F. Wang, I. Grinberg, L. Jiang, S. M. Young, P. K. Davies, A. M. Rappe, *Materials design of visible-light ferroelectric photovoltaics from first principles*, Ferroelectrics, **483**(1), 1-12, (2015).

[15] S. Hao, M. Yao, G. Vitali-Derrien, P. Gemeiner, M. Otoničar, P. Ruello, H. Bouyanfif, P.-E. Janolin, B. Dkhil, C. Paillard, *Optical absorption by design in a ferroelectric: co-doping in $BaTiO_3$*, J. Mater. Chem. C, **10**(1), 227-234, (2022).

[16] M. Irshad, Q. tul Ain, M. Zaman, M. Z. Aslam, N. Kousar, M. Asim, M. Rafique, K. Siraj, A. N. Tabish, M. Usman, et al., *Photocatalysis and perovskite oxide-based materials: a remedy for a clean and sustainable future*, RSC Adv., **12**(12), 7009-7039, (2022).

[17] Z. Li, Y. Sun, H. Zhao, *Enhanced optical properties of lead-free double perovskite $Cs_2AgBiBr_6$ nanocrystals by doping of Na ions*, Solid State Commun., **373**, 115288, (2023).

[18] Z. Chen, S. Zhao, L. Zhou, J. Li, *First-principles investigations on the physical properties of the double perovskite Cs_2OsI_6*, Solid State Commun., **389**, 115556, (2024).

[19] R. Kundara, S. Baghel, *Performance analysis of $LaFeO_3$ perovskite solar cells: A theoretical and experimental study*, Solid State Commun., 115590, (2024).

[20] A. Rajagopal, K. Yao, A. K.-Y. Jen, *Toward perovskite solar cell commercialization: a perspective and research roadmap based on interfacial engineering*, Adv. Mater., **30**(32), 1800455, (2018).

[21] Z. N. Jaf, Z.-T. Jiang, H. A. Miran, M. Altarawneh, J.-P. Veder, M. Minakshi, Z.-f. Zhou, H. N. Lim, N. M. Huang, B. Z. Dlugogorski, *Physico-chemical properties of CrMoN coatings-combined experimental and computational studies*, Thin Solid Films, **693**, 137671, (2020).

[22] H. A. Miran, M. Altarawneh, Z. N. Jaf, M. M. Rahman, M. H. Almatarneh, Z.-T. Jiang, *Influence of the variation in the Hubbard parameter (U) on activation energies of CeO_2-catalysed reactions*, Can. J. Phys., **98**(4), 385-389, (2020).

[23] H. A. Miran, Z. N. Jaf, I. H. Khaleel, A. A. Alkhafaji, *Photocatalytic and optical performances of CeO_2 by substitution of titanium*, Phys. Chem. Res., **9**(4), 553-564, (2021).

[24] X. Guo, Y. Sun, L. Liu, Z. Yu, J. Liu, *Effect of different ionic valence state doping on the structure and characteristic of $BiFeO_3$-$BaTiO_3$-based ceramics*, Int. J. Appl. Ceram. Technol., **21**(3), 1688-1699, (2024).

[25] Md. Moniruddin, B. Ilyassov, X. Zhao, E. Smith, T. Serikov, N. Ibrayev, R. Asmatulu, N. Nuraje, *Recent progress on perovskite materials in photovoltaic and water splitting applications*, Mater. Today Energy, **7**, 246-259, (2018).

[26] B. Sun, G. Zhou, L. Sun, H. Zhao, Y. Chen, F. Yang, Y. Zhao, Q. Song, *ABO_3 multiferroic perovskite materials for memristive memory and neuromorphic computing*, Nanoscale Horiz., **6**(12), 939-970, (2021).

[27] C. J. Rhodes, *Perovskites and their potential use in solar energy applications*, Sci. Prog., **97**(3), 279-287, (2014).

[28] A. Fatima, H. M. Naeem Ullah, M. Rizwan, S. Maqbool, F. Idrees, Z. Usman, *Theoretical description of structural, electronic, elastic, mechanical, and optical response of $Ba_{1-x}Cd_xTiO_3$ for optoelectronic applications*, Mater. Today Commun., **35**, 105925, (2023).

[29] M. Rizwan, H. Naeem, H. M. Naeem Ullah, Z. Usman, N. Amjed, M. Abid, *Fine band gap tuning via Sr incorporated $PbTiO_3$ for optoelectronic application: a DFT study*, Opt. Quantum Electron., **56**(1), 122, (2024).

[30] C. Chen, Q. Ma, F. Liu, J. Gao, X. Li, S. Sun, H. Yao, C. Liu, J. Young, W. Zhang, *Photocatalytically reductive defluorination of perfluorooctanoic acid (PFOA) using $Pt/La_2Ti_2O_7$ nanoplates: experimental and DFT assessment*, J. Hazard. Mater., **419**, 126452, (2021).

[31] Q. Ma, W. Zhang, J. Young, *Effect of single atom platinum (Pt) doping and facet dependent on the electronic structure and light absorption of lanthanum titanium oxide ($La_2Ti_2O_7$): A density functional theory study*, Surf. Sci., **715**, 121949, (2022).

[32] L. Lv, H.-D. Yang, Q.-W. Chen, H. Fan, J.-P. Zhou, *$La_2Ti_2O_7$ nanosheets modified by Pt quantum dots for efficient NO removal avoiding NO_2 secondary pollutant*, Environ. Res., **223**, 115441, (2023).

[33] Z. P. Tshabalala, J. Kano, H. C. Swart, D. E. Motaung, *Influence of Pt-loading on the energy band gap and gas sensing of titanium perovskite*, Physica B Condens. Matter, **676**, 415687, (2024).

[34] M. Q. Saadon, H. A. Miran, *Computational modeling study on the physical properties of Pd doped $BaTiO_3$ perovskite*, Comput. Condens. Matter, **39**, e00906, (2024).

[35] S. J. Clark, M. D. Segall, C. J. Pickard, P. J. Hasnip, M. I. J. Probert, K. Refson, M. C. Payne, *First principles methods using CASTEP*, Z. Kristallogr. Cryst. Mater., **220**(5-6), 567-570, (2005).

[36] M. D. Segall, P. J. D. Lindan, M. J. Probert, C. J. Pickard, P. J. Hasnip, S. J. Clark, M. C. Payne, *First-principles simulation: ideas, illustrations and the CASTEP code*, J. Phys. Condens. Matter, **14**(11), 2717, (2002).

[37] J. P. Perdew, K. Burke, M. Ernzerhof, *Generalized Gradient Approximation Made Simple*, Phys. Rev. Lett., **77**(18), 3865-3868, (1996).

[38] J. P. Perdew, K. Burke, Y. Wang, *Generalized gradient approximation for the exchange-correlation hole of a many-electron system*, Phys. Rev. B, **54**(23), 16533-16539, (1996).

[39] H. J. Monkhorst, J. D. Pack, *Special points for Brillouin-zone integrations*, Phys. Rev. B, **13**(12), 5188-5192, (1976).

[40] M. G. Brik, *First-principles study of the electronic and optical properties of $CuXS_2$ (X = Al, Ga, In) and $AgGaS_2$ ternary compounds*, J. Phys. Condens. Matter, **21**(48), 485502, (2009).

[41] H. A. Miran, Z. N. Jaf, M. Altarawneh, M. M. Rahman, A. T. Al-Bayati, E. M.-T. Salman, *First-principles analysis of Cr-doped $SrTiO_3$ perovskite as optoelectronic materials*, Iran. J. Mater. Sci. Eng., **20**(1), (2023).

[42] Muhammad Rizwan, Adnan Ali, Zahid Usman, N. R. Khalid, H. B. Jin, and C. B. Cao, *Structural, electronic and optical properties of copper-doped $SrTiO_3$ perovskite: A DFT study*, Physica B: Condensed Matter, **552**, 52–57, (2019).

[43] A. Rached, M. A. Wederni, K. Khirouni, S. Alaya, R. J. Martín-Palma, and J. Dhahri, *Structural, optical and electrical properties of barium titanate*, Mater. Chem. Phys., **267**, 124600, (2021).

[44] Mohammed Tihtih, Jamal Eldin F. M. Ibrahim, Mohamed A. Basyooni, Walid Belaid, László A. Gömze, and István Kocserha, *Structural, optical, and electronic properties of barium titanate: experiment characterization and first-principles study*, Mater. Tech., **37**(14), 2995–3005, (2022).

[45] Fan Yang, Liang Yang, Changzhi Ai, Pengcheng Xie, Shiwei Lin, Cai-Zhuang Wang, and Xihong Lu, *Tailoring bandgap of perovskite $BaTiO_3$ by transition metals co-doping for visible-light photoelectrical applications: A first-principles study*, Nanomaterials, **8**(7), (2018).

[46] Mohammed Tihtih, Jamal-Eldin Ibrahim, M. A. Basyooni-M. Kabatas, Redouane Ennadir, Walid Belaid, Mohamed Abdelfattah, Irina Hussainova, Gábor Pszota, and István Kocserha, *Enhanced optical and thermal conductivity properties of barium titanate ceramic via strontium doping for thermo-optical applications*, Opt. Quantum Electron., **55**, 226, (2023).

[47] *Ferroelectric-like metallic state in electron-doped $BaTiO_3$*, Sci. Rep., **5**, (2015).

[48] Zainab N. Jaf, Hussein A. Miran, Imad H. Khaleel, and Kareem A. Jasim, *Assessing the optoelectronic performance of d-orbital doped cubic HfO_2: The case of W, Nb, and Mo*, Optik, **264**, 169341, (2022).

[49] Lihong Yang, Hongmei Qiu, Liqing Pan, Zhengang Guo, Mei Xu, Jinhua Yin, and Xuedan Zhao, *Magnetic properties of $BaTiO_3$ and $BaTi_{1-x}M_xO_3$ (M = Co, Fe) nanocrystals by hydrothermal method*, J. Magn. Magn. Mater., **350**, 1–5, (2014).

[50] Md. Atikur Rahman, Md Rahman, and Zahidur Rahaman, *First-principles calculations of structural, electronic and optical properties of $HfZn_2$*, J. Adv. Phys., **5**, 354–358, (2015).

[51] Daniel Sanchez-Portal, Emilio Artacho, and Jose M. Soler, *Projection of plane-wave calculations into atomic orbitals*, Solid State Commun., **95**(10), 685–690, (1995).

[52] Ram Kinkar Roy, Kimihiko Hirao, Sailaja Krishnamurty, and Sourav Pal, *Mulliken population analysis based evaluation of condensed Fukui function indices using fractional molecular charge*, J. Chem. Phys., **115**, 2901–2907, (2001).

[53] Ramon Carbó-Dorca and Patrick Bultinck, *Quantum mechanical basis for Mulliken population analysis*, J. Math. Chem., **36**, 231–239, (2004).

[54] Wei Jiang, Zhiyong Gao, Wei Sun, Jiande Gao, and Yuehua Hu, *A Density Functional Theory Study on the Effect of Lattice Impurities on the Electronic Structures and Reactivity of Fluorite*, Minerals, **7**(9), (2017).

[55] Yang Wang, Qinyan Zhou, Qiankai Zhang, Yuanyang Ren, Kunqi Cui, Chuanhui Cheng, and Kai Wu, *Effects of La-N Co-Doping of $BaTiO_3$ on Its Electron-Optical Properties for Photocatalysis: A DFT Study*, Molecules, **29**(10), (2024).

[56] M. G. Brik, *First-principles calculations of electronic, optical and elastic properties of $ZnAl_2S_4$ and $ZnGa_2O_4$*, J. Phys. Chem. Solids, **71**(10), 1435–1442, (2010).

[57] R. K. Goyal, S. S. Katkade, and D. M. Mule, *Dielectric, mechanical and thermal properties of polymer/$BaTiO_3$ composites for embedded capacitor*, Compos. B Eng., **44**(1), 128–132, (2013).

[58] Zainab N. Jaf, Hussein A. Miran, M. Mahbubur Rahman, Amun Amri, and Zhong-Tao Jiang, *DFT + U investigation on high-pressure properties of monoclinic CuO*, Can. J. Phys., **102**(5), 316–323, (2024).

[59] Azmat Iqbal, Madiha Batool, Sikander Azam, and Amin Rahman, *First-principles quantum computational study to investigate radiation energy-dependent effect on optoelectronic properties of bismuth oxyhalides BiOX (X = I, Br)*, Radiat. Phys. Chem., **221**, 111775, (2024).

[60] Asif Nadeem, Azmat Iqbal, Sikander Azam, Amin Rahman, and Muhammad Iqbal, *Cd-doping-assisted tuning of transparency and conductivity of $MnIn_2O_4$ by density functional quantum theoretical approach*, Eur. Phys. J. Plus, **328**, (2023).

[61] Ji Chen, Shanshan Hu, Shining Zhu, and Tao Li, *Metamaterials: From fundamental physics to intelligent design*, Interdisciplinary Materials, **2**, (2022).

[62] Zainab N. Jaf, Zhong-Tao Jiang, Hussein A. Miran, and Mohammednoor K. Altarawneh, *Thermo-elastic and optical properties of molybdenum nitride*, Can. J. Phys., **94**, 902–912, (2016).

[63] Hussein A. Miran and Zainab N. Jaf, *Electronic and optical properties of nickel-doped ceria: A computational modelling study*, Papers in Physics, **14**, 140002, (2022).

[64] Azmat Iqbal, Syeda Batool, Ayesha Arif, and Asim Shazad, *Dispersion-dependent superluminal propagation and photon drag in GaAs/AlGaAs quantum dot molecule*, Phys. Scr., **98**, (2023).

[65] Xihong H., *A review on the dielectric materials for high energy-storage application*, J. Adv. Dielectr., **3**(1), 1330001, (2013).